Early View publication on
www.wileyonlinelibrary.com
(issue and page numbers not yet assigned;
citable using Digital Object Identifier – **DOI**)

J. Biophotonics 1–9 (2012) / **DOI** 10.1002/jbio.201200169

Journal of
BIOPHOTONICS

FULL ARTICLE

Quantitative analysis of dynamic behavior of osteoblasts during in vitro formation of micro-mass cell cultures

Susanne Schäfer[1], *Markus Dekiff*[2], *Ulrich Plate*[1], *Thomas Szuwart*[1], *Cornelia Denz*[3], *and Dieter Dirksen*[*,2]

[1] University of Münster, Dept. of Maxillofacial Surgery, Germany
[2] University of Münster, Dept. of Prosthetic Dentistry and Biomaterials, Waldeyerstr. 30, 48149 Münster, Germany
[3] University of Münster, Institute of Applied Physics, Germany

Received 29 August 2012, revised 21 September 2012, accepted 22 September 2012
Published online 1 November 2012

Key words: tissue engineering, osteoblasts, cell tracking, cell micro-masses, multicellular spheroids

Improvements in bone tissue engineering require an understanding of cellular and tissue level behavior of osteoblast-like cells. Experiments indicate that in the absence of an anchoring material, intercellular adhesion may be based on signals that promote cell activity resulting in the formation of a spheroid cell-matrix. The aim of the present study is to investigate the formation of scaffold-free three-dimensional micro-mass cell spheroids in vitro, and to characterize quantitatively the cell movement. A new correlation based automated tracking method is evaluated in order to optimize the processing parameters and to identify statistical parameters that characterize the cell behavior. Results suggest that the temporal development of the mean distance of the cells to the center of gravity may be described by an exponential function, thus providing a characteristic time constant as a quantitative measure of cell dynamics.

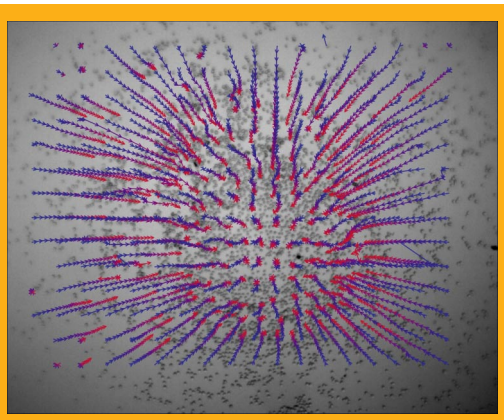

Trajectories of osteoblasts forming a micro-mass spheroid obtained by correlation tracking.

1. Introduction

Bone defects and deformities are common sequels of congenital development, trauma or surgical ablation therapy [1–3]. New therapeutic approaches for bone regeneration basically require a comprehensive understanding of the cellular and tissue level mechanisms that underlie bone healing. To improve bone tissue engineering strategies, it is of utmost importance to mimic the native developmental mechanisms of bone growth and differentiation. The proliferative and osteogenic potential of bone-cells of the periosteum can be used to produce bone-like tissue ex vivo, e.g. in order to regenerate lost bone.

Whereas most studies on extracorporeal tissue engineering are based on the use of scaffold material

* Corresponding author: e-mail: dirksdi@uni-muenster.de, Phone: (+49) 251 83 56825; Fax: (+49) 251 83 47182

[4, 5], scaffold-free tissue engineering implicates significant advantages. An overview of scaffold-free cell based therapies in regenerative medicine is given by Kelm and Fussenegger [6]. As an example, in the absence of an anchoring material, intercellular adhesion may be based on signals that promote cell activity [7]. By the aid of the non-attachment feature of agarose, it is possible to form cell aggregates rich in extracellular matrix (ECM). The principle of such a cell aggregation is to prevent cell adhesion to a culture surface, which forces adherent-dependent cells, like osteoblasts, to reform into tissue. These cell micro-masses formed by the osteoblast-like cells have features of bone tissue with respect to the formation of the ECM complexes and the development of the cells from primary cell generation up to formed cell micro-mass cultures, the cell spheroids (spheres). Langenbach et al. showed that osteogenic differentiation of three-dimensional (3-D) cell micro-masses is enhanced by mimicking in-vivo conditions [8]. Because of an increased ECM synthesis, micro-masses are more adhesive than cultures in a two-dimensional monolayer [9]. Out of these reasons, these cell micro-masses are implemented in the present study.

However, a thorough understanding of the process of cell migration during sphere formation, is lacking until now. Especially, the automated tracking of osteoblasts by digital image processing algorithms is challenging due to the fact that in the present case individual cells often can hardly be differentiated.

For the automated tracking of individual cells in two or three dimensions, a huge variety of approaches and implementations of cell tracking exists [10–12]. A cell tracking process can be divided into two steps. First, the cells have to be recognized and separated from the background. For this step, the so-called segmentation, several methods exist that implement e.g. thresholding, watershed transformation, template matching [13], or deformable models [14]. In the second step, corresponding cells are identified in subsequent images. Features like cell positions, areas/volumes, orientations, and intensities can be used to find the closest match for each investigated cell. Some approaches are based on template matching [12, 15], and more sophisticated methods exploit e.g., estimated cell dynamics [14] or probabilistic schemes [13].

The aim of the presented study is to generate scaffold-free 3-D micro-mass cell spheroids in vitro and to characterize and evaluate quantitatively the movement of the cells during 3-D cell-micro-mass formation by a novel cell tracking algorithm. For this purpose, an image processing software has been developed that allows image acquisition as well as the quantitative evaluation of cell motion.

In order to find adequate parameters that describe sphere formation, individual cell movements are of minor interest. Thus, instead of trying to identify and track single cells as most of the previously described algorithms do, we developed an alternative approach based on two-dimensional image correlation techniques. By applying this method, statistical information on the dynamics of multi-cell structures during sphere formation is obtained. Parameters describing the dynamics of this process like the center of gravity (CoG), the mean velocity, and the mean distance to the CoG are calculated as time-depending functions. Results of manual and automated tracking are compared in order to optimize the processing parameters and to identify characteristic statistical parameters that describe the cell behavior.

2. Materials and methods

2.1. Cell culture for micro-mass formation

For culture, the potential of osteoblasts to migrate from periosteum explants is used [16]. The periosteal layer of calf metacarpus is aseptically stripped off the bone, cut into small pieces and plated into polystyrene culture dishes (15 cm in diameter) with their osteogenic side facing the bottom of the dishes. 500 ml High Growth Enhancement Medium (MP Biomedicals GmbH, Leiden, The Netherlands) supplemented with 60 ml fetal calf serum 690, 5 ml amphotericin B, 5 ml penicillin/streptomycin and 5 ml L-glutamine (Biochrom KG seromed, Berlin, Germany) is used for culture maintenance and replaced once a week. The cultures are incubated at 37 °C in a humidified atmosphere of 95% air and 5% CO_2.

Culture conditions and cell proliferation are routinely checked by light microscopy (Diaphot-TMD, Nikon Kogaku K. K., Tokyo, Japan). A confluent monolayer is obtained in about three weeks. Bovine primary osteoblast-like cells are detached by accutase incubation (PAA Laboratories GmbH Pasching, Austria). While a sample volume of 100 µl is counted in a Casy-counter system (CASY I Model TT, Schaerfe System GmbH, Reutlingen, Germany) with 10 ml CasyTon, the remaining solution is centrifuged for 10 minutes at 600 rpm. Finally, resuspension is carried out with 1 ml of a Leibovitz medium per 1 million cells. Micro-masses (spheroids) are generated by cultivating cells in a non-attachment environment (Figure 1). 1% agarose (Biozym Scientific GmbH, Hess. Oldendorf, Germany)-coated 1 µ-slide angiogenesis Ibidi treat chambers (Ibidi, Martinsried, Germany) are prepared by applying 5 µl of a warm mixture of 10 ml Leibovitz (Gibco® invitrogen GmbH, Karlsruhe, Germany) and 0.1 g agarose (Biozym Scientific GmbH, Hess. Oldendorf, Germany) in one well which is then stored at 4 °C. The thickness of the resulting agarose layer is estimated to 0.4 mm. Osteoblasts are transferred into the pre-

formed non-attachment agarose coated 1 µ-slide angiogenesis Ibidi treat. 50 µl of the harvested primary osteoblast suspension at a density of 0.1 million cells/ml of medium is inoculated in each well. The wells are then placed in a heating stage (Ibidi, Martinsried, Germany) at 37 °C. First passage cells were used as indicated for all experiments. Phenotypic characterization of osteoblasts revealed the expression of osteonectin und collagen I.

2.2. Image acquisition and analysis

For image acquisition and analysis, a specialized software has been developed using the programming language C# (Microsoft Visual Studio 2010), and free numerical libraries (OpenCV [17] and FFTW [18]). Image acquisition is performed via the Microsoft DirectShow interface of Windows XP. Thus, different cameras with drivers which are compatible to the Windows Driver Model (WDM) can be used. In the present case, an USB color camera (TC 131 USB Cam, Tucsen Ltd, Fuzhou, China) with a resolution of 1280 × 1024 pixels is attached to the camera port of the microscope (Diaphot-TMD, Nikon, Tokyo, Japan). The used objective is a PL 2.5 ×/0.08 −170/-PL (Leitz, Wetzlar, Germany). Controlled by a notebook (operating system: Windows XP), sequences of single RGB images are recorded with adjustable time delays in between. The elapsed time is coded as part of the file names. Additional information, like the image scale, is stored in a project description file. In order to minimize the accumulated amount of data a programmable time delay between subsequent image recordings is employed.

2.2.1 Manual cell tracking

In order to provide reference data for the automated tracking routine described later, a simple interactive tool for manual cell tracking has been implemented. The program allows the user to mark individual cell positions in a sequence of images where the cell identities are represented by consecutive numbers. After the cell positions have been transformed from pixel to metric coordinates, individual trajectories are stored in a text file as sequences of paired coordinates and time values (in seconds).

2.2.2 Automated tracking of cell structures

The automated cell tracking employs a technique called Digital Image Correlation (DIC), which is an established method to determine displacement fields in experimental mechanics [19, 20]. DIC requires a digital image depicting the initial state of the specimen and an image depicting the displaced state. One image is defined as reference image (e.g. the image depicting the initial state) and divided into (usually square) small regions, so-called subimages, which are then sought-after in the other image, the so-called search image. The displacement at the center point of one of those subimages is defined as the difference between the point's image coordinates in the reference image and the image coordinates of the center of the corresponding subimage in the search image. The critical task during this procedure is actually finding the corresponding subimage. Therefore, usually different subimages of the search image are compared to the subimage in the reference image. A similarity measure has to be calculated for each combination of subimages. The subimage in the search image which yields the highest similarity value is assumed to correspond to the subimage from the reference image. In case of large deformations of the object more advanced, computationally intensive correspondence search algorithms that take account of the expected deformations are required.

The DIC algorithm we use to find correspondences in different images of cells is lent from Electronic (or Digital) Speckle Photography (ESP/DSP) [21, 22] where it is employed to find corresponding subimages in digital images of speckle patterns that are formed by an object's surface while being illuminated by a laser. The evaluation of the recorded image sequence depicting the cell migration is carried out successively. First, the first image of the sequence represents the reference image and the second the search image, then the second image becomes the reference image (with subimages locations specified by the previous evaluation step) and the third one the search image, and so forth. The similarity measure is given by the two-dimensional correlation coefficient:

$$c(k,l)=\sum_{i=\frac{m-1}{2}}^{\frac{m-1}{2}}\sum_{J=\frac{m-1}{2}}^{\frac{m-1}{2}}[I_1(u+i,\,v+j)\,I_2(u+i+k,\,v+j+l)] \tag{1}$$

where u and v denote the pixel coordinates of the subimage center in the reference image, $u+k$ and $v+l$ denote the pixel coordinates of the center of a subimage in the search image, m is the (odd) width and height of the (square) subimage, I_1 and I_2 represent the intensity distributions of the reference and search image, respectively. The aim is to find those values for k and l that maximize $c(k,l)$.

The calculation is more efficient in the spectral domain. Hence, instead of Eq. (1)

$$\mathbf{C}=F^{-1}(H_{s2}^{*}H_{s1}) \tag{2}$$

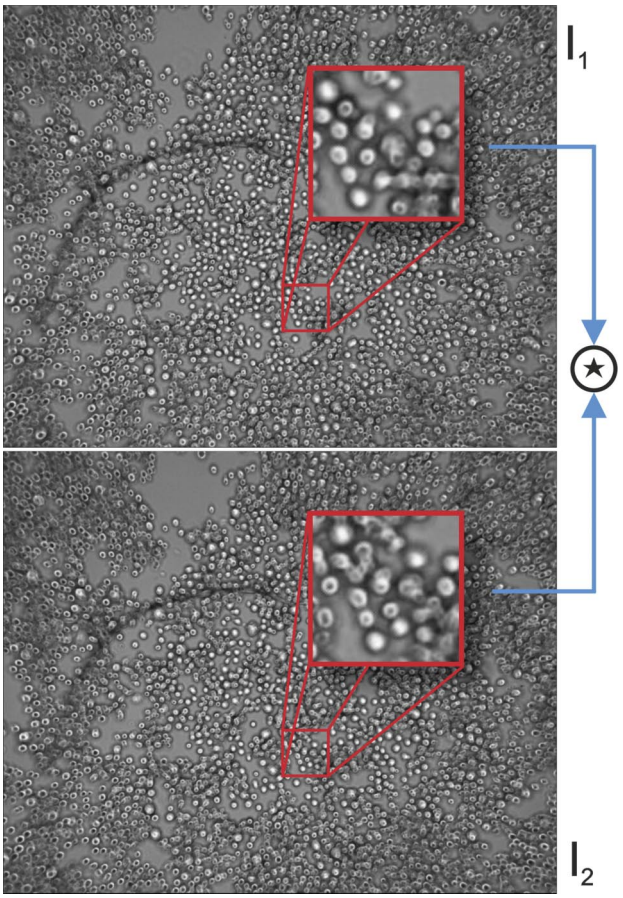

Figure 1 (online color at: www.biophotonics-journal.org) Details of two subsequently recorded microscope images of osteoblasts. The red squares depict enlargements of two corresponding subimages (99 × 99 pixel) that are used for correlation analysis. Original image size: 1280 × 1024 pixel, scale: 1.71 μm/pixel.

is evaluated, where **C** is the cross correlation matrix, containing all $c(k,l)$ for $k,l = -\frac{m-1}{2}, -\frac{m-1}{2}+1, ..., \frac{m-1}{2}$, F^{-1} denotes the inverse (fast) Fourier transform and H_{s1} and H_{s2} represent the Fourier transforms of the subimages from the reference and search image (both with their centers at (u,v)). Finding the translation between both subimages (± 0.5 pixel) is subsequently only a matter of determining the position of the maximum of **C**. In this way, only translations up to $\frac{m-1}{2}$ pixels can be determined by this algorithm. If larger translations are expected, it is necessary to calculate Eq. (2) for various subimages from the search image or to increase the subimage size m.

H_{s1} and H_{s2} have to be padded to twice their size before performing the calculation of **C**, which is done best by subtracting the respective mean value from the subimages and padding them with zeros. Iterating the calculation of **C** with a new subimage from the search image at the previously estimated location can yield a better defined peak in **C**.

There are several ways of improving the algorithm to achieve subpixel accuracy (e.g., by fitting a continuous function to the peak region of **C** and determining the location of its maximum), but in our application case this is not supposed to be necessary. It has to be noted that in contrast to manual tracking which allows determining the trajectories of individual cells, our automated cell tracking analyses the average motion of all cells contained in a subimage (Figures 1 and 2).

2.2.3 *Evaluation of cell dynamics*

From the recorded trajectories, three basic statistical parameters are calculated for each (discrete) time step t_k: the center of gravity (CoG) r_s, the mean velocity $\bar{v}$, and the mean distance d_s to the CoG.

$$r_s(t_k) = \frac{1}{N}\sum_{i=1}^{N} r_i(t_k) \tag{3}$$

$$\bar{v}(t_k) = \frac{1}{N}\sum_{i=1}^{N} \frac{|r_i(t_{k+1}) - r_i(t_k)|}{t_{k+1} - t_k} \tag{4}$$

$$d_s(t_k) = \frac{1}{N}\sum_{i=1}^{N} |r_i(t_k) - r_s(t_k)| \tag{5}$$

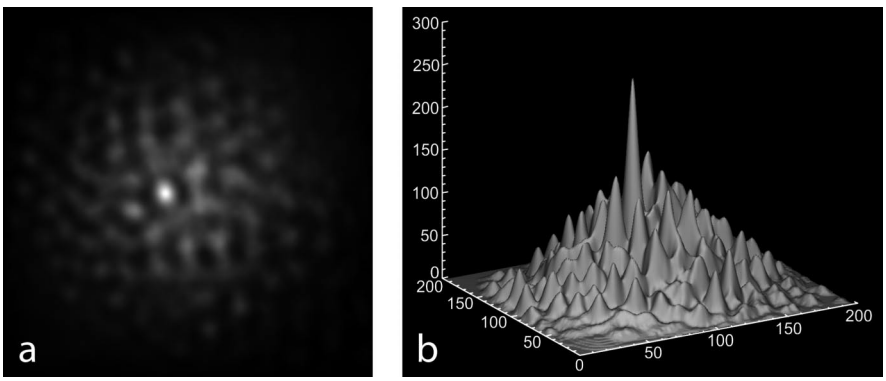

Figure 2 The two-dimensional correlation function **C**. (**a**) intensity plot, (**b**) pseudo 3-D plot calculated for the regions marked in Figure 1 by Eq. (2). The position of its maximum indicates a translation of 12 pixels in horizontal direction.

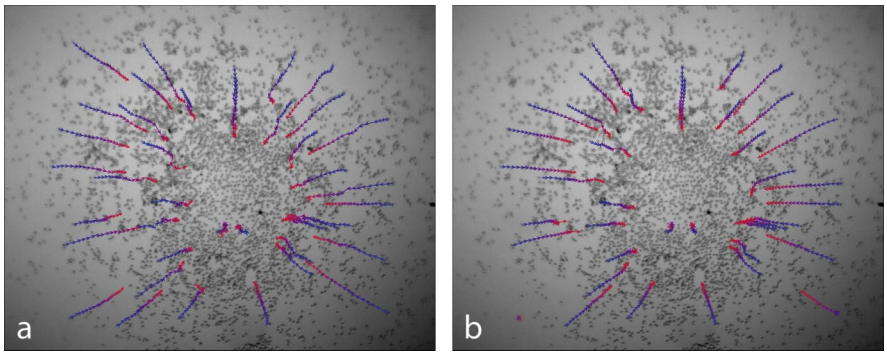

Figure 3 (online color at: www.biophotonics-journal.org) Comparison of manual tracking (**a**) and automatic tracking (**b**). Trajectories of 40 cell positions are evaluated. Cell trajectories start at the peripheral (blue) ends. Original image size: 1280 × 1024 pixel, scale: 1.97 μm/pixel.

Here, $r_i(t_k) = (x_i, y_i)$ denotes the position vector of a cell (or cell pattern in the case of correlation) within the k^{th} frame (i.e. at time t_k).

In the preceding formulas summations are carried out over all N marked positions at a certain time step (i.e. a frame). As not all tracked cells may be identified in all frames, N may change from frame to frame.

3. Results

The following results are obtained with a single culture of 5,000 osteoblasts produced and cultivated as described above. After approximately one hour, a compact micro-mass structure has formed. A sequence of 20 images is recorded with a time delay of 1 min between subsequent exposures. The sequence has been limited to this length in order to allow a manual evaluation for comparison.

3.1 Comparison of manual and automated tracking

For manual evaluation, a set of 40 cell positions is chosen in the peripheral region of the developing micro-mass agglomeration (Figure 3a). Start positions are subsequently adopted as initial positions of the correlation process. The result is displayed in Figure 3b. A comparison of Figures 3a and b reveals nearly identical tracks. Minor differences can be found e.g. in the upper and lower left corners, where two tracks could not be found by the automatic analysis.

An important parameter that influences the results of automatic tracking is the width of the subimages (windows) for which the local displacements are calculated by correlation. Windows that are either too small or too large may lead to a strong decrease in the number of identified cell positions. Thus, automatic tracking results for five different subimage sizes are compared to a result obtained by manual tracking.

In Figure 4 the mean velocities (according to Eq. (4)) for these cases are displayed. Note that each data point represents a mean of about 40 cell velocities. Therefore, when comparing the curves, standard deviations have to be considered. These have not been added to the graph for the sake of clarity, but they are displayed for a similar situation (i.e. the same image sequence) in Figure 7. They show that all curves are within the 2σ margins. As there appears to be no clear tendency with respect to the used window size (within the chosen limits), any of these seem to be applicable.

Figure 5 depicts the temporal evolution of the mean distances of cell positions (within a frame) to the center of gravity for manually as well as for automatically evaluated tracks. Again, there is no clear tendency of the deviation from the manually acquired tracks with respect to the window size. The difference between the curves of both methods is somewhat growing over time which is not too surprising as – in contrast to manual evaluation – the correlation function describes the average shift of a

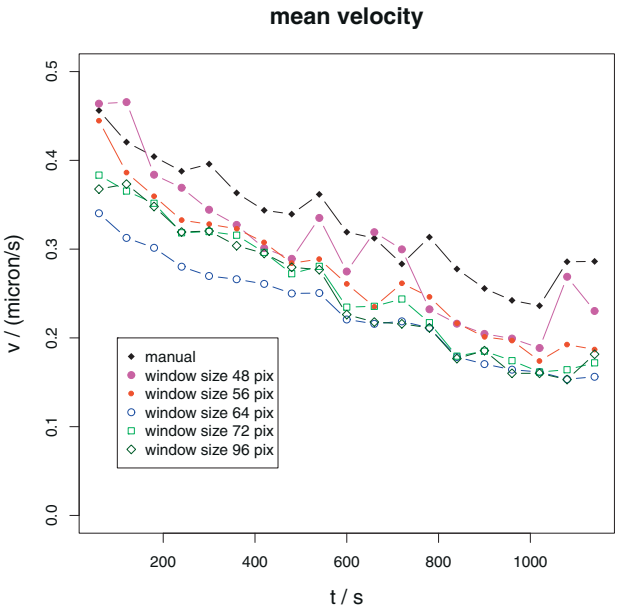

Figure 4 (online color at: www.biophotonics-journal.org) Mean velocity calculated by Eq. (3) from the tracked cell positions in each frame.

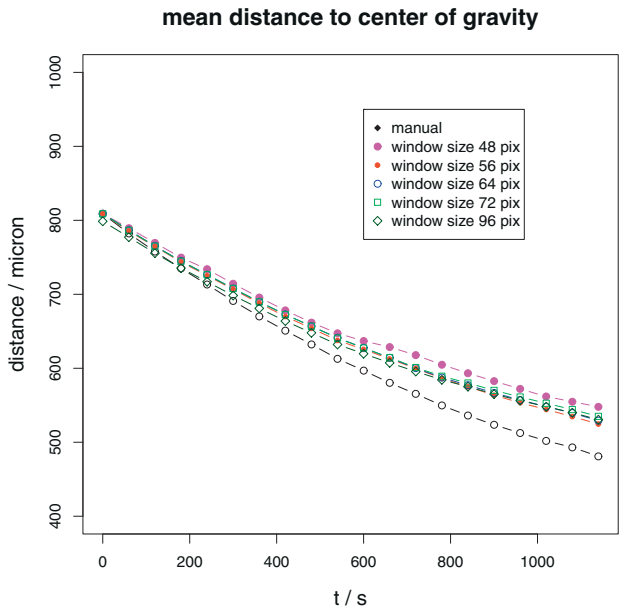

Figure 5 (online color at: www.biophotonics-journal.org) Mean distance to center of gravity calculated by Eq. (5) from the tracked cell positions in each frame.

cell ensemble. Differences are again smaller than the respective error interval (see also Figure 8).

3.2 *Automated analysis of cell dynamics*

For the regular evaluation of the osteoblast movement, the same parameters are calculated for the identical image sequence as in the example shown before. In contrast, the start positions of the correlation windows are now located on a regular grid of which the grid spacing can be adjusted. In the presented case a window size of 64×64 pixels and a grid spacing of 64 pixels (in both horizontal and vertical direction) have been chosen. Computation takes about 2 s per image on a desktop system with an Intel core i7 processor.

In Figure 6 the calculated trajectories for the image sequence with a duration of 20 min are displayed. A total number of 252 trajectories have been detected. Nearly all of the tracks show an inbound radial direction. On the one hand, those starting in the peripheral region are generally longer (≈ 400 µm), indicating that the corresponding cells are moving faster. On the other hand, cells located in the central region are hardly moving at all. The center of gravity remains almost at a fixed position (total displacement ≈ 50 µm).

The mean velocity for each frame as a function of time is depicted in Figure 7 with 2σ intervals. It demonstrates that the osteoblasts are moving faster at the beginning of the formation process ($\bar{v} \approx 0.34$ µm/s) than at the end ($\bar{v} \approx 0.16$ µm/s). The standard deviation is quite large ($\sigma \approx 1.5$ µm/s) which reflects the differences in velocity between cells in central and peripheral regions.

Figure 8 shows the mean distances to the center of gravity calculated from the trajectories in Figure 6 with 2σ intervals. These intervals mainly reflect the geometrical situation, i.e. by defining that the peripheral cells are located farther from the center of gravity than the central ones. Despite of the large standard deviation ($\sigma \approx 260$ µm), the mean distance

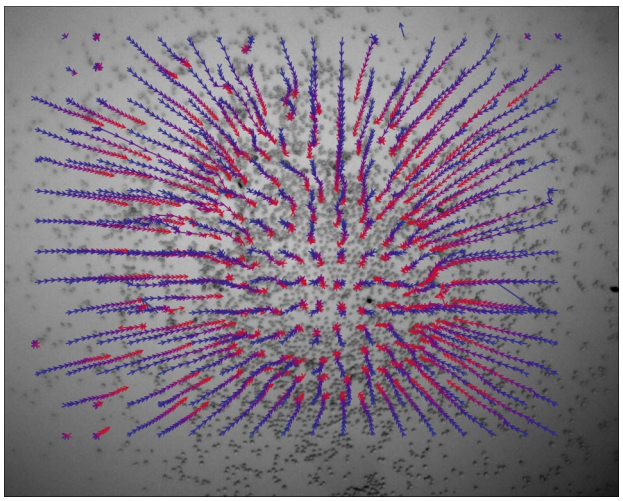

Figure 6 (online color at: www.biophotonics-journal.org) Trajectories found by correlation tracking using a subimage size of 64×64 pixels and a grid spacing of 64×64 pixels. Original image size: 1280×1024 pixel, scale: 1.97 µm/pixel.

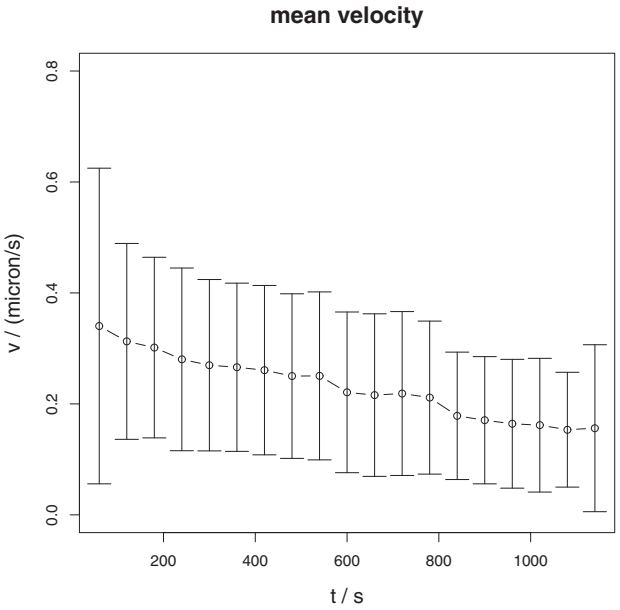

Figure 7 Mean velocity calculated from trajectories in Figure 6 with 2σ error.

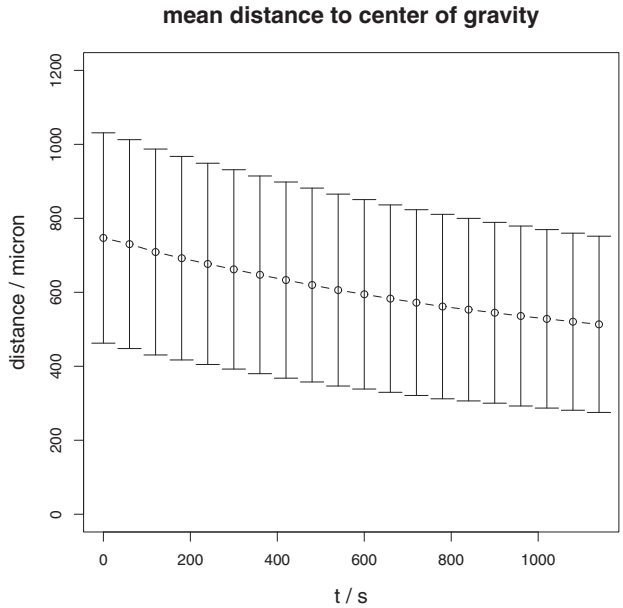

Figure 8 Mean distances to the center of gravity calculated from trajectories in Figure 6 with 2σ error.

evolves as a smooth function of time, starting at ≈ 750 μm and ending at ≈ 510 μm.

The monotony and continuity of the curve inspire fitting of an analytical function, and the overall shape suggests an exponential approach. The result of a nonlinear least squares fit (accomplished with the gnls function of the statistical package *R* [23]) is displayed in Figure 9. The exponential function (time constant $\tau \approx 1100$ s, offset $b_1 \approx 370$ μm) fits the data with a residual standard error of less than one micron.

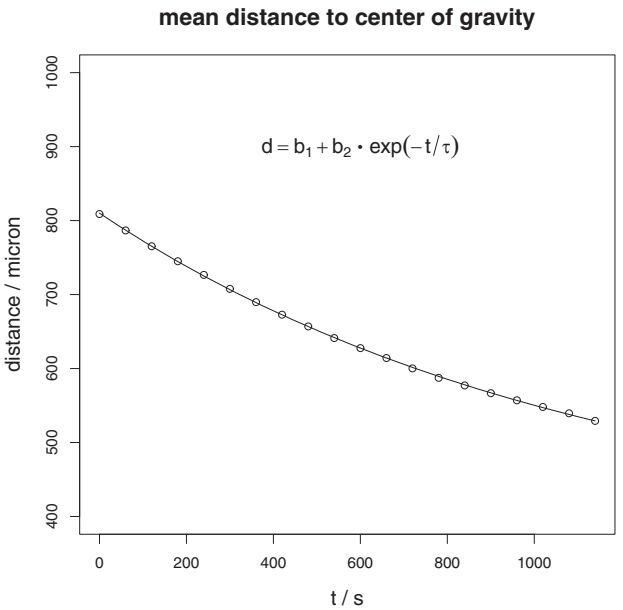

Figure 9 Mean distances to the center of gravity calculated from trajectories in Figure 6 as a function of time with least squares fit of exponential function ($b_1 = 370.1$ μm, standard error SE = 5.12 μm; $b_2 = 439.4$ μm, SE = 4.84 μm; $\tau = 1118$ s, SE = 21.2 μm, residual standard error: 0.96 μm).

4. Discussion and conclusion

Progress in osteogenic tissue engineering requires a thorough understanding of cellular interactions of osteoblast-like cells. However, even basic questions as if and how cell activity is controlled by signals are still unanswered. Scaffold-free tissue engineering with bovine osteoblasts, as it has been employed here, allows an insight into the cell dynamics during formation of micro-masses or spheres. For this purpose, parameters are required that allow a quantitative description of the dynamic behavior as well as adequate tools to measure them.

For an approach, which describes the behavior of the cell culture as an ensemble, the dynamics of a single cell is of little significance. Thus, we propose statistical methods both for acquisition and description. A new method of cell tracking is proposed which is based on correlation analysis of multi-cell structures rather than on identifying and tracking single cells. In comparison to the methods for automated tracking of individual cells mentioned in the introduction, our approach is quite simple, yet has proven to be effective. It has the advantage of being able to deal with situations in which individual objects (e.g. cells) are hard to identify as has been shown for other applications [24]. The result is a set of trajectories of cells or cell patterns that may extend over a varying number of image frames.

Two statistical parameters to characterize the cell dynamics have been investigated: the mean velocity calculated for these trajectories during each frame, and the mean distance to the center of gravity. In order to verify the results of the correlation analysis, these have been compared to results obtained by manually tracking single cells. Within the statistical error margins, the curves are in good agreement.

The fully automatic evaluation of an image sequence of a cell culture consisting of 5,000 osteoblasts resulted in approximately 250 individual trajectories. Both, the mean velocity and the mean distance to the center of gravity decrease in a characteristic way during the observation time (Figures 7 and 8). The standard deviations of both parameters are relatively large. This is probably due to the fact that the velocity as well as the distance to the CoG is not uniformly distributed. At least with respect to the geometrical distribution of the cells this is obvious (Figure 6). However, both parameters seem to behave – as functions of time – in a monotonic and smooth way. In case of the mean distance to the CoG, an exponential function can be fitted that is in

agreement with the data. Further investigations will have to proof whether this can be generalized to other experimental configurations. First results indicate that such a generalization is justified. For this case, the corresponding time constant (here: 1100 s) is a simple parameter to characterize the dynamic behavior of osteoblast-like cells.

Moreover, we are convinced that our image processing software of automated cell tracking is also a useful tool of documentation for other models of sphere-generation, like neurospheres, chondrospheres, or myocardial microspheres. Cell migration to form spheres in turn is an adequate means to create the required cell mass and will impact the therapeutic potential of the cells.

Acknowledgment Financial support of the Arbeitsgemeinschaft Elektronenoptik, Germany, is gratefully acknowledged.

Susanne Schäfer did her diploma at the University of Applied Sciences in Münster, Germany, in oecotrophology. She is currently studying medical science at the University of Münster. Her doctoral thesis focuses on the optical and biochemical analysis of micro-mass cultures of bone tissue cells.

Markus Dekiff obtained his diploma degree in physics from the University of Münster, Germany. He is currently doing his doctorate at the same university. His research focuses on optical shape and deformation measurement techniques as well as on finite element analyses of biomaterials.

Ulrich Plate obtained his Ph.D. in physics at the University of Münster, Germany and worked as a postdoc at the Institute of Medical Physics and Biophysics. As an associate researcher he works at the Section of Tissue Engineering and Biomineralization, Dept. of Cranio-Maxilliofacial Surgery, University of Münster. His research focuses on basic and applied investigations in tissue engineering, biomineralization, implantology and bone (re)generation.

Thomas Szuwart studied biology at the University of Münster, Germany. He did his Ph.D. on structural and biochemical study of the ossification process of bone tissue at the Zoologisches Institut, University of Münster and worked as a postdoc in the area of platelet stimulation and bone formation at the Institute of Anatomy, University of Münster. Since 2010 he works in the Biomineralisation Research Unit, Department of Cranio-Maxillofacial Surgery, University of Münster.

Cornelia Denz received her Ph.D. from Darmstadt University of Technology, Germany. In 1992 she received the Lise Meitner-Award, and in 1999 the Adolf-Messer-Award for her work in optical neural networks and nonlinear dynamic phase contrast microscopy, respectively. Since 2001, she is a director of the Institute of Applied Physics and head of the Nonlinear Photonics group at University of Münster, Germany. Her main research interests are on the application of nonlinear optics and photonics in information technology and life sciences. Cornelia Denz is a fellow of the Optical Society of America and the European Optical Society.

Dieter Dirksen studied physics at the University of Oldenburg, Germany, and obtained his Ph.D. from the University of Osnabrück, Germany. He completed his Habilitation at the University of Münster, Germany, where he is currently working as head of the Material Science Section at the Dept. of Prosthetic Dentistry and Biomaterials. His research focuses on the application of non-destructive optical measurement methods on biomaterials.

References

[1] D. A. Atwood and J. Prosthet. Dent. **26**, 266–279 (1971).
[2] A. Tallgren and J. Prosthet. Dent. **27**, 120–132 (1972).
[3] J. I. Cawood and R. A. Howell, Int. J. Oral Maxillofac. Surg. **17**, 232–236 (1988).
[4] E. G. Khaled, M. Saleh, S. Hindocha, M. Griffin, and W. S. Khan, Open Orthop. J. 5 Suppl. **2**, 289–295 (2011).
[5] M. Vallet-Regí, I. Izquierdo-Barba, and M. Colilla, Philos Transact A Math. Phys. Eng. Sci. **370**, 1400–1421 (2012).
[6] J. M. Kelm and M. Fussenegger, Adv. Drug Deliv. Rev. **62**, 753–764 (2010).
[7] R. C. Bates, N. S. Edwards, and J. D. Yates, Crit. Rev. Oncol. Hematol. **36**, 61–74 (2000).
[8] F. Langenbach, C. Naujoks, R. Smeets, K. Berr, R. Depprich, N. Kübler, and J. Handschel, Clin. Oral Investig (Online First, DOI: 10.1007/s00784–012-0763–8) (2012).
[9] J. M. Kelm, V. Lorber, J. G. Snedeker, D. Schmidt, A. Broggini-Tenzer, M. Weisstanner, B. Odermatt, A. Mol, G. Zünd, and S. P. Hoerstrup, J. Biotechnol. **148**, 46–55 (2010).
[10] E. Meijering, O. Dzyubachyk, and I. Smal, Meth. Enzymol. **504**, 183–200 (2012).
[11] E. Meijering, I. Smal, O. Dzyubachyk, and J. Olivo-Marin, in: Microscope Image Processing, Q. Wu, F. A. Merchant, and K. R. Castleman (eds.) (Academic Press, Burlington, 2008), pp. 401–440.
[12] A. J. Hand, T. Sun, D. C. Barber, D. R. Hose, and S. MacNeil, J. Microsc. **234**, 62–79 (2009).
[13] N. N. Kachouie, P. Fieguth, J. Ramunas, and E. Jervis, Int. J. Biomed. Imag. **2006**, 1–10 (2006).
[14] O. Debeir, I. Camby, R. Kiss, P. Van Ham, and C. Decaestecker, Cytometry A **60**, 29–40 (2004).
[15] C. A. Wilson and J. A. Theriot, IEEE Trans. Image Process. **15**, 1939–1951 (2006).
[16] S. J. Jones and A. Boyde, Cell Tissue Res. **184**, 179–193 (1977).
[17] http://opencv.org/
[18] M. Frigo and S. G. Johnson, Proc. IEEE **93**, 216–231 (2005).
[19] T. Chu, W. Ranson, and M. Sutton, Exp. Mech. **25**, 232–244 (1985).
[20] M. A. Sutton, J.-J. Orteu, and H. Schreier, Image Correlation for Shape, Motion and Deformation Measurements (Springer, New York, 2009).
[21] M. Sjödahl and L. R. Benckert, Appl. Opt. **32**, 2278–2284 (1993).
[22] M. Sjödahl, Appl. Opt. **29**, 125–144 (1998).
[23] http://www.r-project.org/
[24] M. Dekiff, P. Berssenbrügge, B. Kemper, C. Denz, and D. Dirksen, Appl. Phys. B **99**, 449–456 (2010).